Simulation of prepreg platelet compression molding: Method and orientation validation

Anthony J. Favaloro, Drew E. Sommer, Benjamin R. Denos, and R. Byron Pipes

Citation: Journal of Rheology **62**, 1443 (2018); doi: 10.1122/1.5044533
View online: https://doi.org/10.1122/1.5044533
View Table of Contents: https://sor.scitation.org/toc/jor/62/6
Published by the The Society of Rheology

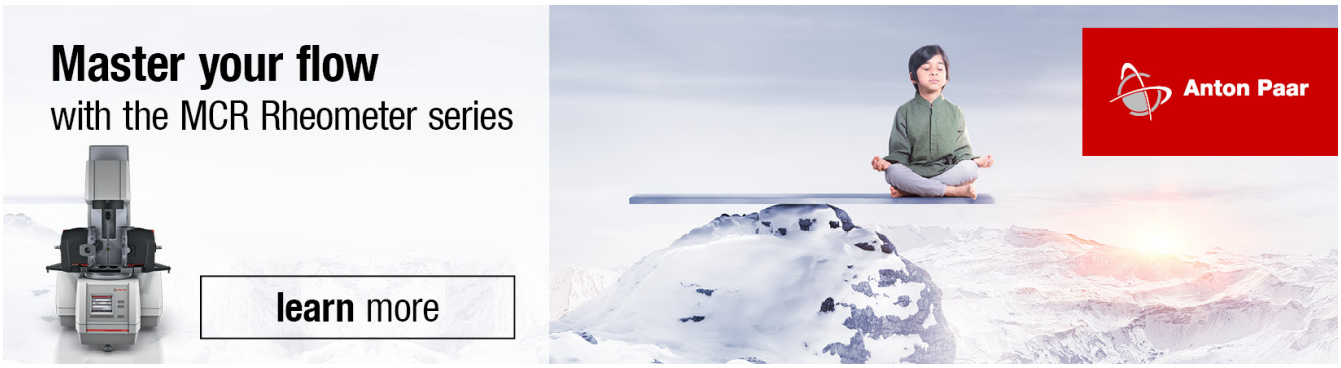

Simulation of prepreg platelet compression molding: Method and orientation validation

Anthony J. Favaloro,[a] Drew E. Sommer, Benjamin R. Denos, and R. Byron Pipes

Composites Manufacturing and Simulation Center, Purdue University, West Lafayette, Indiana 47906

(Received 13 June 2018; final revision received 17 September 2018; published 10 October 2018)

Abstract

Prepreg platelet molding compounds (PPMCs) offer improved performance potential as compared to short-fiber composites and increased geometrical complexity as compared to continuous fiber composites. The increased adoption of PPMCs in automotive and aerospace applications necessitates the development of predictive tools for determining the final orientation state in complex geometries produced through molding flows. Due to the large geometric scale of platelets as compared to molded geometry scales, the orientation structure of PPMCs is spatially nonsmooth, thereby eliminating the requisite separation of scales utilized by typical molding simulation approaches. Additionally, the large fiber volume fraction and fiber length in platelets yield highly anisotropic flow behavior, as manifested in the resistance to stretching deformations along platelet fiber directions. Thus, the goal of this work is to present the development, implementation, and validation of a flow simulation approach for PPMCs accounting for fiber direction and platelet normal direction evolution with coupled anisotropic viscous behavior. The simulation approach is implemented using the smoothed particle hydrodynamics method. To validate the proposed approach, a pin bracket geometry is manufactured from a charge with the orientation state measured by computed tomography (CT). The final orientation state determined by the flow simulation predictions and by measuring the orientation state of the final bracket by CT is compared to validate the predictions. © *2018 The Society of Rheology.* https://doi.org/10.1122/1.5044533

I. INTRODUCTION

The mechanical performance of polymer matrix composite molded geometries is highly dependent upon the fiber length and the fiber orientation state [1]. In the case of continuous fibers, high-performance properties are achieved through directly prescribing desired orientation states. However, the complexity of permissible molded geometries, wherein the fiber orientation can be controlled, is quite limited. In contrast, short- and long-fiber injection molding systems offer ease of processing but provide only relatively low-performance properties due to discontinuous fibers and flow-induced orientation structures. Prepreg platelet molding compounds (PPMCs) offer an intermediate solution in which significant fiber length and fiber volume fraction are achieved in a material system which can be molded into moderately complex geometries. However, the mechanical performance of molded geometries is similarly dictated by the flow-induced orientation structure. PPMCs are formed by slitting and cutting prepreg tape to a prescribed length and width while the platelets inherit the thickness of the prepreg tape. When the polymer matrix is a thermoplastic, platelets may be stored loose; when the matrix is a thermoset, platelets are typically formed into a flat sheet or mat form. No additional matrix material is added to the system. In this way, PPMCs reach large fiber volume fractions, typically 50–60%. The PPMC is then used in compression or transfer molding processes to mold complex geometries. Figure 1 shows the prepreg tape product (a), resulting platelet elements (b), and a complex molded PPMC geometry, a pin bracket (c). Geometries produced with PPMCs have low void content [2,3] but present interplatelet resin rich regions. The authors have not observed fiber breakage in the inspection of molded geometries.

PPMCs possess three scales of interest: the molded geometry scale, the platelet scale, and the fiber scale. Typically, platelet lengths are greater than part thicknesses. From the micrograph of the pin bracket cross section shown in Fig. 2, the platelet scale can clearly be seen as compared to the pin bracket with the mesostructure in some regions strongly resembling that of laminated, continuous fiber composites. The near scale similarity between the platelet scale and typical part thickness results in spatially nonsmooth orientation structures. While performance analysis of PPMCs is an active research topic, a review of many preliminary efforts can be found in Ref. [4]. In the early approaches, the orientation state is taken as planar and uniform random. Details on the performance of the bracket geometry considered in this work can be found in Ref. [5]. One major result of the performance research showed that while the linear elastic performance of PPMCs may be treated as locally transversely isotropic, due to the formation of features such as the knitline seen in Fig. 2(a) and the laminate-like mesostructure seen in Fig. 2(c), PPMCs require a three-dimensional description of damage in which platelet through-thickness properties can vary significantly from in-plane properties. Thus, an outcome of a relevant flow simulation must contain both the fiber direction and platelet normal direction orientation state in order to describe local material properties.

While limited research has been performed on the processing of PPMCs, notably by Hubert and coworkers [3,6–9],

[a]Author to whom correspondence should be addressed; electronic mail: afavalor@purdue.edu

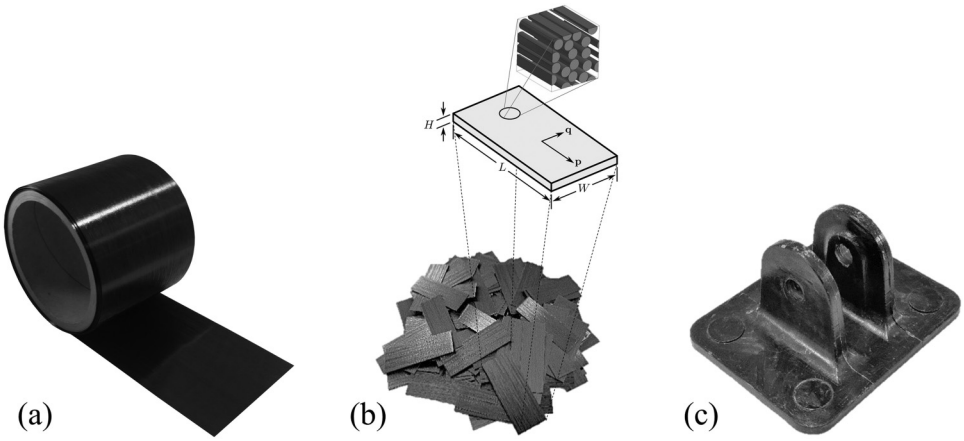

FIG. 1. PPMC process: (a) prepreg tape, (b) slit and cut into platelet form, and (c) compression molded into a bracket.

the evolution of orientation state has not been a particular topic of focus. However, the orientation state in PPMCs directly influences the effective performance [5,10,11]. Thus, predictive simulations are required in order to understand the development of mesostructural features and aid in the design process of both the material system and the molding process. In developing such a simulation framework, careful attention must be taken to ensure that an orientation state useful for performance simulations is described and determined. Additionally, due to the significant fiber length and volume fraction of PPMCs, the flow of the system is highly anisotropic. To address this requirement herein, the authors take a coupled orientation analysis and anisotropic viscous flow simulation approach.

In this study, the focus is on the prediction of the final mesostructure of a molded geometry, particularly the platelet fiber and platelet normal directions. A coupled anisotropic viscosity and orientation evolution simulation method is developed in which commercial finite element analysis software, namely, ABAQUS/EXPLICIT, is utilized in conjunction with the smoothed particle hydrodynamics (SPH) methods and user subroutines. In this way, a Lagrangian simulation approach capable of large deformation analysis is utilized in order to maintain the spatial variability of PPMCs due to the significance of the platelet scale as compared to the molded geometry scale. The current implementation is an extension of previous work by the authors in which a numerical approach for coupled anisotropic viscosity and orientation evolution was implemented in ABAQUS/STANDARD for the simulation of anisotropic squeeze flow [12]. The simulation predictions are validated by comparisons of orientation state determined by computed tomography (CT) scan analysis. Unlike previous approaches, wherein the initial orientation state is taken as in-plane uniform random, the orientation state in an initial charge is determined by CT scan analysis methods [13] and taken as the initial condition of the simulation. The material system used in this work is an aerospace-grade carbon fiber thermoplastic.

II. MODEL DEVELOPMENT

A. Orientation representation and evolution

To perform a coupled orientation analysis and anisotropic flow simulation, an orientation representation method, an orientation evolution method, and an orientation dependent constitutive model are required. Each component of the model must be consistent with the previously described prepreg platelet molded geometry scale considerations. The orientation state of a platelet is described by four unit vectors: the fiber direction, $\mathbf{p}$, a nonorthogonal in-plane direction, $\hat{\mathbf{q}}$, an orthogonal in-plane direction, $\mathbf{q}$, and the platelet normal direction, $\mathbf{r}$. Under the assumption of affine motion of fiber

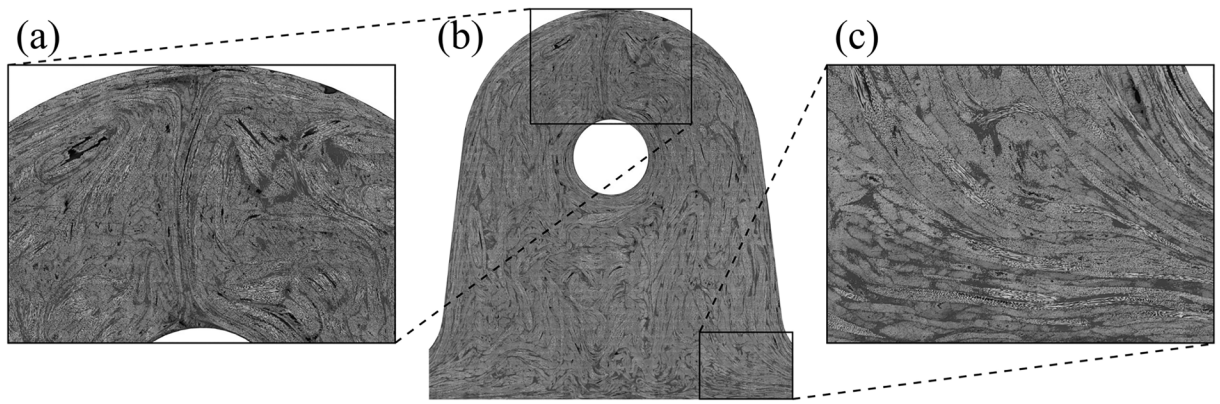

FIG. 2. Bracket cross-section micrograph: (a) knit-line mesostructure, (b) flange cross section, and (c) laminate-like mesostructure.

orientation and the nonorthogonal in-plane direction, as will be taken, $\mathbf{p}$ and $\hat{\mathbf{q}}$ are the minimum, independent set of directions as $\mathbf{q}$ may be determined through orthogonalization of $\hat{\mathbf{q}}$ with respect to $\mathbf{p}$, and $\mathbf{r}$ is given simply as $\mathbf{r} = \mathbf{p} \times \mathbf{q}$. A diagram of the four vectors is shown in Fig. 3. Clearly, by tracking $\mathbf{p}$ and $\hat{\mathbf{q}}$, slightly more information than orientation is determined as the shearing angle of the platelet is also determined. Misalignment between $\hat{\mathbf{q}}$ and $\mathbf{q}$ indicates a total amount of shearing experienced by the platelet in the $\mathbf{p}$–$\mathbf{q}$ plane. In the remainder of this work, the fiber direction and platelet normal direction will be the primary concerns.

Orientation evolution in this work will be performed by assuming that the fiber orientation vector, $\mathbf{p}$, and the nonorthogonal in-plane direction vector, $\hat{\mathbf{q}}$, transform affinely in the flow as material lines. In contrast, orientation evolution in conventional molding simulation is performed through a combination of Jeffery's hydrodynamic solution [14], rotary diffusion to account for fiber–fiber interactions [15–18], and reduced orientation kinetics which account for an apparent time scale difference between theoretical orientation evolution and observed orientation evolution [19–21]. Further, these models have been developed considering the fiber scale to be significantly lower than the molded geometry scale. However, the near fitting of platelets may lead to restriction of the motion of surrounding platelets to be conforming with their motion. Affine motion is a conforming motion. Such restricted motion has been referred to as "caging" by Tucker and Advani in Ref. [22] in the discussion of the reduction of interaction coefficient for the Folgar–Tucker model as fiber volume fraction and aspect ratio increase. Thus, at the platelet scale, orientation diffusion and reduced orientation kinetics are neglected in this investigation; rather, the only platelet-to-platelet interaction in the model is implicit through anisotropic viscosity and spatially varying orientation state captured at the simulated macroscale. The assumption of affine motion yields the fiber orientation of a platelet resulting from a given deformation gradient, $\mathbf{F}_{ij} = \partial \mathbf{x}_i / \partial \mathbf{x}_j^0$, with an initial fiber orientation, $\mathbf{p}^0$, as

$$\mathbf{p} = \frac{\mathbf{F} \cdot \mathbf{p}^0}{\|\mathbf{F} \cdot \mathbf{p}^0\|}. \tag{1}$$

The nonorthogonal in-plane direction, $\hat{\mathbf{q}}$, evolves according to Eq. (1) as well. The resulting platelet normal direction after a given deformation gradient from the initial normal direction, $\mathbf{r}^0$, is then given as

$$\mathbf{r} = \frac{\mathbf{F}^{-T} \cdot \mathbf{r}^0}{\|\mathbf{F}^{-T} \cdot \mathbf{r}^0\|}. \tag{2}$$

When expressed as material derivatives, Eqs. (1) and (2) take the following forms:

$$\dot{\mathbf{p}} = \mathbf{L} \cdot \mathbf{p} - \mathbf{L} : \mathbf{ppp} = \mathbf{W} \cdot \mathbf{p} + (\mathbf{D} \cdot \mathbf{p} - \mathbf{D} : \mathbf{ppp}), \tag{3}$$

$$\dot{\mathbf{r}} = -\mathbf{L}^T \cdot \mathbf{r} + \mathbf{L}^T : \mathbf{rrr} = \mathbf{W} \cdot \mathbf{r} - (\mathbf{D} \cdot \mathbf{r} - \mathbf{D} : \mathbf{rrr}), \tag{4}$$

where $\mathbf{L} = \dot{\mathbf{F}} \cdot \mathbf{F}^{-1}$ is the velocity gradient tensor, $\mathbf{W} = (\mathbf{L} - \mathbf{L}^T)/2$ is the vorticity tensor, and $\mathbf{D} = (\mathbf{L} + \mathbf{L}^T)/2$ is the rate-of-deformation tensor. Here, it is clearly seen that Eqs. (3) and (4) correspond exactly to Jeffery's equation [14,23] in the limiting cases of infinitely long particles and infinitely thin disks, respectively. Thus, the assumption of affine motion is equivalent to Jeffery's equation for infinite length fibers, for the fiber direction vector, and Jeffery's equation for infinitely thin disks, for the normal direction vector. From Eqs. (3) and (4), the orientation tensor approach introduced by Advani and Tucker [24] could be taken. Orientation tensors are a concise representation of an orientation distribution function. However, in the present work, an orientation distribution function cannot represent the prepreg platelet material system due to the finite character of the heterogeneity. Thus, the present approach (i.e., the considered geometry scale and platelet scale similarity) is unable to utilize the advantages of tensor-based methods: namely, low variable count and well-defined algebraic averaging allowing Eulerian methods. Without well-defined algebraic averaging of the orientation state, as is the case with physically meaningful orientation vectors, orientation calculations must be performed in a Lagrangian framework. Nevertheless, orientation tensors provide a convenient postprocessing metric through which the orientation state in specific volumes is compared. Thus, we define the second- and fourth-order fiber orientation tensors as $\mathbf{A} = \langle \mathbf{pp} \rangle$ and $\mathbb{A} = \langle \mathbf{pppp} \rangle$, where $\langle\ \rangle$ indicates a volume averaging of the quantity over the orientation state [24], and we define the second- and fourth-order platelet normal orientation tensors as $\mathbf{N} = \langle \mathbf{rr} \rangle$ and $\mathbb{N} = \langle \mathbf{rrrr} \rangle$, respectively.

While the relative scales of the present investigation are such that orientation tensor-based methods are inappropriate, PPMCs may be used to produce geometries which are quite large compared to the platelet scale. In such cases, element sizes used in numerical methods may be large enough to contain a plurality of platelets improving the appropriateness of orientation tensors as the primary orientation descriptor. For completeness, the authors demonstrate the use of the presented orientation model (both fiber directions and normal directions) in a typical flow using orientation tensor-based methods in the Appendix.

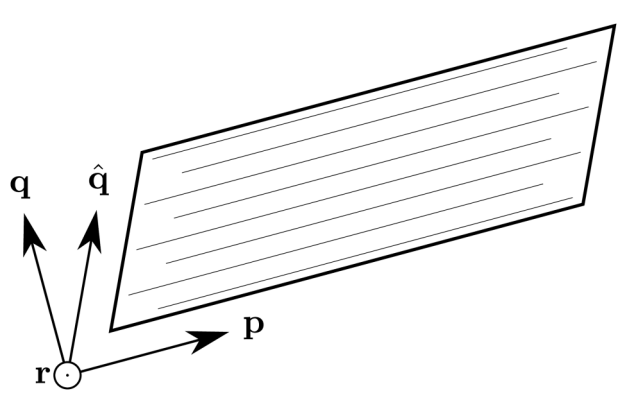

FIG. 3. Platelet orientation vectors.

B. Anisotropic viscosity

The effect of reinforcing fibers on the response of suspensions is a well-studied problem [25–28]. Herein, the constitutive relation for a platelet is taken as viscous and transversely

isotropic [29,30], owing to the microstructure of each platelet consisting of a collimated fiber suspension of high fiber volume fraction. Following the notation of Beaussart *et al.* [31], three viscosities must be investigated: the extensional viscosity in the fiber direction, η_{11}, the in-plane shearing viscosity, η_{12}, and the transverse shearing viscosity, η_{23}. For collimated fiber suspensions, Pipes *et al.* [28] determine $\eta_{12} \approx \eta_{23} = \kappa\eta_0$, where η_0 is the neat matrix shearing viscosity and $\kappa^{-1} = 1 - \sqrt{V_f/F}$ is a shape factor related to interfiber spacing or fiber volume fraction given a fiber arrangement, and $F = \pi/\sqrt{12}$ for hexagonal packing. For a 60% volume fraction system, κ is approximately 5.36 indicating only a moderate increase in shearing viscosity as compared to the neat matrix. For a fiber suspension, the extensional viscosity is related to the square of the fiber aspect ratio, $(L_f/D_f)^2$ [25–28]. Due to the continuity of fibers within a platelet, viscous extension of the platelet does not occur. Rather, concentrated platelet suspensions develop extensional viscosity due to platelet-to-platelet interactions behaving similar to fiber suspensions with the effective diameter being the platelet thickness. Therefore, the extensional viscosity is related to the square of the platelet length-to-thickness ratio, $(L/H)^2$ [29,30,32]. This ratio dominates when the platelet width is much larger than the thickness such that the stress transfer between platelets occurs at platelet surfaces. In contrast, the effective shearing viscosity terms of the platelet system, η_{12} and η_{23}, are of the same order as the embedded fiber suspension. Thus, the effective extensional viscosity of the platelet system is several orders of magnitude greater than the neat matrix viscosity. With $\eta_{12} = \eta_{23}$ (as in the work of Pipes *et al.* [28]) and defining an anisotropy ratio, $R_\eta = \eta_{11}/\eta_{22} = (\eta_{11}/\eta_{23} + 1)/4$, the fourth-order anisotropic viscosity tensor can be written as:

$$\langle\eta\rangle_{ijkl} = 4\eta_{23}(R_\eta - 1)\left[\mathbb{A}_{ijkl} - \frac{1}{3}\left(\mathbf{A}_{ij}\mathbf{I}_{kl} + \mathbf{A}_{kl}\mathbf{I}_{ij} - \frac{1}{3}\mathbf{I}_{ij}\mathbf{I}_{kl}\right)\right] + 2\eta_{23}\left[\frac{1}{2}(\mathbf{I}_{ik}\mathbf{I}_{jl} + \mathbf{I}_{il}\mathbf{I}_{jk}) - \frac{1}{3}(\mathbf{I}_{ij}\mathbf{I}_{kl})\right], \tag{5}$$

where $\mathbf{I}$ is the second-order identity tensor. Equation (5) is the result of orientation averaging [24] the generalized inverse [33] of the viscous compliance matrix of Beaussart *et al.* [31]. While this expression allows for the viscosity to be determined as an orientation average, in this work, it simply serves to transform the transversely isotropic constitutive relationship into the global coordinate system. Using Eq. (5), the deviatoric stress is determined simply as $\boldsymbol{\tau} = \langle\eta\rangle : \mathbf{D}$. When incompressibility of the suspension can be assumed, $\mathrm{tr}(\mathbf{D}) = 0$, the constitutive relationship reduces to

$$\tau = 4\eta_{23}(R_\eta - 1)[\mathbb{A} - \mathbf{IA}/3] : \mathbf{D} + 2\eta_{23}\mathbf{D}. \tag{6}$$

This relationship is equivalent to that of Dinh and Armstrong [26] and used by Tucker [34] with the exception that using Eq. (5) produces a deviatoric stress rather than an extra stress as required by the numerical implementation outlined in Sec. III B. Clearly, for an anisotropy ratio of unity, $R_\eta = 1$, Eq. (6) reduces to the constitutive relationship of a Newtonian fluid, while for a large anisotropy ratio as is the case considered in this work, $R_\eta \gg 1$, the first term is dominant. In the simple case of lubricated squeeze flow, as considered in Refs. [12,35], for sufficiently large $R_\eta (R_\eta \gtrsim 1000)$, the orientation solution is insensitive to the value of R_η due to the convergence of the velocity field. Here, we note that while the full platelet coordinate system is considered throughout the analysis, only the fiber direction orientation state is significant for the proposed constitutive model.

The anisotropic behavior of PPMCs has been verified in a simple compression molding center-gated disk (CGD) as shown in Fig. 4. An initial charge was preconsolidated with a collimated initial orientation state ($\mathbf{A}_{11} \approx 1$, $\mathbf{N}_{33} \approx 1$). The collimated charge was then used in a short shot molding of the CGD geometry. Under the assumption of an isotropic constitutive model, the predicted shape of the flow front of a short shot would be a circle. However, as seen in Fig. 4(c), nearly all deformation occurs transverse to the initial fiber direction. This result implies a large anisotropy ratio, R_η, as the resistance to stretching in the fiber direction far exceed the resistance transverse to the fibers.

III. EXPERIMENTAL AND NUMERICAL METHODS

A. Experimental procedure

Determining a representative initial orientation state is nontrivial due to the uncontrolled nature of PPMCs in which charges are prepared often by simply pouring loose platelets into a charge cavity. While stochastic methods for orientation state initialization can be taken, comparisons between physical orientation states and simulated orientation state are difficult to assess due to the inherent variability. To examine actual flow

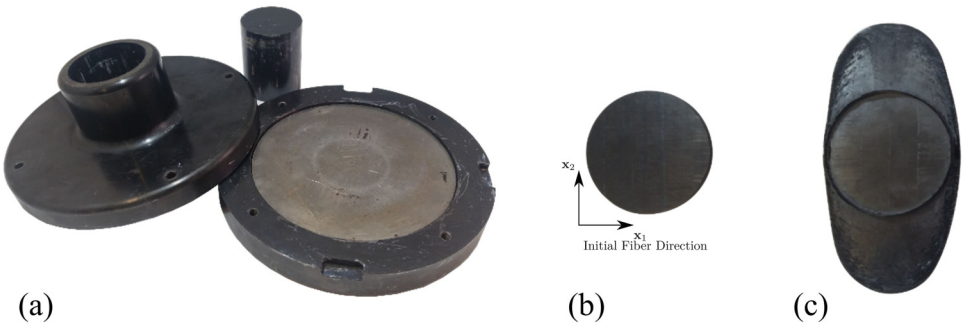

FIG. 4. Compression molding CGD demonstrating anisotropic flow: (a) CGD tool, (b) initial charge, and (c) short shot.

orientation and compare to simulation results, the following procedure is undertaken: manufacture a preconsolidated charge using a consolidation tool the same dimensions as the pin bracket tool charge cavity, CT scan the molded preform, and perform fiber and platelet normal orientation analysis [11] on the resulting charge to serve as initial conditions for the flow simulation. Next, a bracket geometry is molded using the preconsolidated charge and CT scan the molded geometry so that an orientation analysis may be performed on the molded part.

Orientation analysis is performed directly on the voxel mesh of the CT scan data. At each point in the volume, the structure tensor is formed from the dyadic product of density gradients in a small neighboring volume. Eigenanalysis of the structure tensor then reveals the directions of maximum, intermediate, and minimum density gradient. The direction of minimum density gradient is taken as the fiber direction, and the direction of maximum density gradient is taken as the normal direction. Minimum density gradient implies that the direction remains within a platelet moving along fiber lengths, while maximum density gradient implies that the direction crosses platelet boundaries. As the platelet width is significantly larger than the thickness, crossing the platelet boundary corresponds to the normal direction. This CT scan analysis method is available for the entire geometry of the bracket from a single scan due to the large platelet scale [13]. A similar initialization approach has been taken recently for fiber suspensions by Song *et al.* [36] using the commercial software MOLDEX3D, though the orientation comparisons are not one-to-one as the simulation initialization is from a separate charge than was molded.

Loose platelets were poured into the preform mold charge cavity, the temperature was raised above the thermoplastic matrix melt temperature and the preform mold was transferred to a press where 55 bar was applied to the ram to produce the consolidated preform. After CT scanning, the consolidated preform was placed in the pin bracket tool, reheated uniformly above melt temperature, and molded into the final part shape with 110 bar of pressure before being cooled and CT scanned. Again, the CT scan based orientation analysis benefits from the scale of the platelets which is used to correlate inter- and intraplatelet density gradients to fiber orientation and platelet normal directions. The final molded geometry is shown in Fig. 1(c). The workflow described for the preconsolidated charge is shown in Fig. 5 from the tooling (a) to the orientation state on the SPH domain (f) ready for simulation. The orientation state information can be seen being transformed and manipulated from a simple photograph of the surface (c), to a slice of the CT scan data near the same surface (d), to the orientation analysis results from the CT scan analysis (e), and to the orientation state from CT scan analysis mapped in a nearest-neighbor mapping onto the SPH domain (f).

B. Numerical procedure

The fully coupled constitutive model described earlier is implemented numerically in ABAQUS/EXPLICIT using a VUMAT in which the orientation state is updated at each time step in response to the deformation gradient using Eqs. (1) and (2) with the incremental deformation gradient. The deviatoric stress is calculated using Eq. (5) with the strain rate approximated as the strain increment over the time increment. While the previous work of the authors in implementing a similar fully coupled viscous constitutive model in ABAQUS/IMPLICIT using a UMAT was limited to simple problems without the extreme deformations encountered in molding, this earlier approach benefitted from incompressible

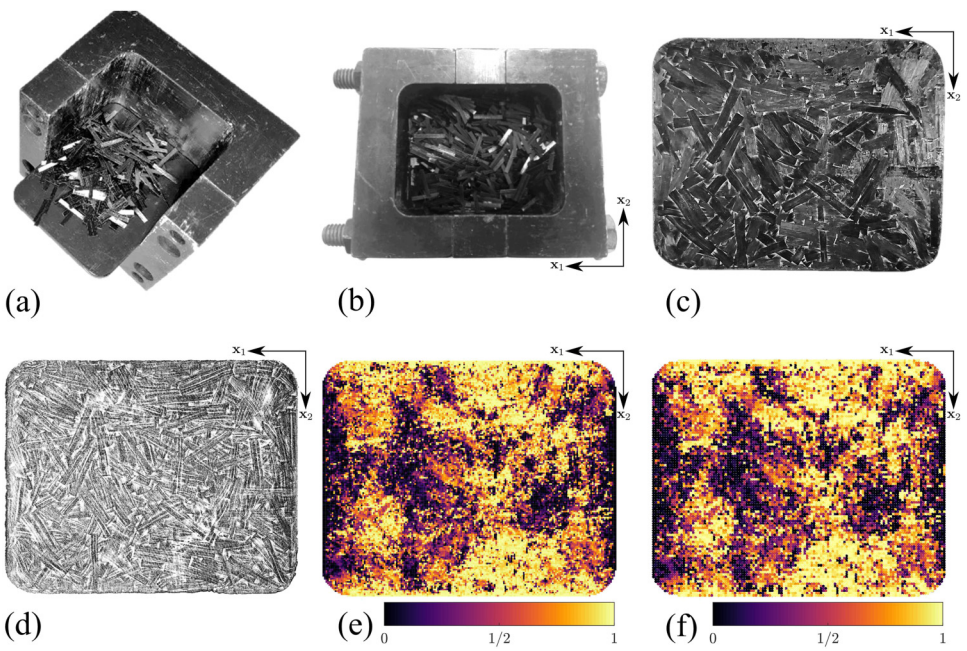

FIG. 5. Preconsolidated preform workflow: (a) partially disassembled tool showing charge cavity, (b) assembled tool with poured platelets, (c) photograph of the cavity-side surface of the consolidated preform, (d) CT scan density field near the cavity-side surface, (e) orientation analysis result on the cavity-side surface, $\mathbf{p}_1^2$, and (f) $\mathbf{p}_1^2$ as mapped onto the SPH domain on the cavity-side surface.

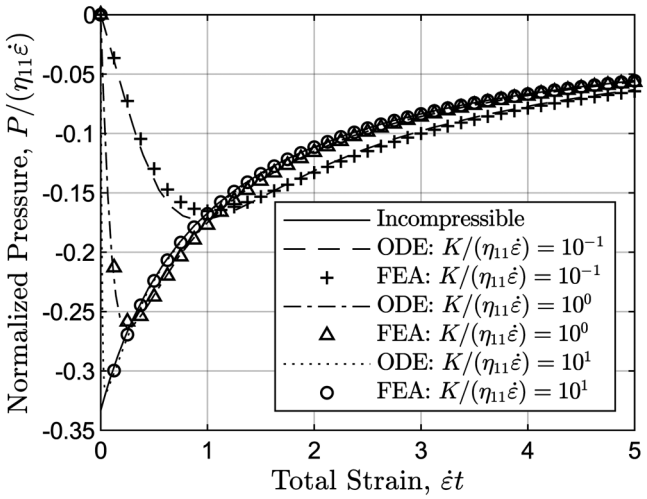

FIG. 6. Pressure lag solution.

element formulations [12]; however, explicit solutions require a finite bulk modulus for a nonzero stable time increment. Thus, the total stress tensor is calculated with the addition of pressure determined by a bulk modulus, K, used as a numerical penalty to enforce near incompressibility as describedbelow:

$$\boldsymbol{\sigma} = \langle \eta \rangle : \frac{\Delta \boldsymbol{\varepsilon}}{\Delta t} + K[\det \mathbf{F} - 1]\mathbf{I}. \tag{7}$$

To assess the effects of the relaxation of incompressibility and develop a heuristic for determining the appropriate penalizing bulk modulus, K, we solve the simple problem of uniaxial extension ($\mathbf{F}_{22} = \mathbf{F}_{33}$) for all fibers aligned in the global $\mathbf{x}_1$-direction. In this way, the deformation does not result in orientation evolution and the effect of the bulk modulus is isolated. The simple ordinary differential equation governing this deformation is given as:

$$\mathbf{F}_{11}\mathbf{F}_{22}^2 - 1 = \frac{2}{9}\left(\frac{\eta_{11}}{K}\right)\left(\frac{\dot{\mathbf{F}}_{11}}{\mathbf{F}_{11}} - \frac{\dot{\mathbf{F}}_{22}}{\mathbf{F}_{22}}\right). \tag{8}$$

In the fully incompressible case ($K \to \infty$), we have $\mathbf{F}_{22} = 1/\sqrt{\mathbf{F}_{11}}$ and the pressure is determined as

$$P = -\frac{1}{3}\eta_{11}\frac{\dot{\mathbf{F}}_{11}}{\mathbf{F}_{11}}. \tag{9}$$

Applying a deformation history in the $\mathbf{x}_1$-direction as $\mathbf{F}_{11} = 1 + \dot{\varepsilon}t$, $\mathbf{F}_{22}$ can be determined and, thereby, the pressure for the nearly incompressible case. In Fig. 6, the resulting pressure solution is developed through directly solving Eq. (8) and using the developed VUMAT in ABAQUS/EXPLICIT for a single C3D8 element. Here, it should be noted that when the bulk modulus is an order of magnitude greater than the viscous stress, the pressure solution for the nearly incompressible constitutive model is nearly identical to the fully incompressible model. This analysis and result serves as a heuristic for tuning the modeling parameter K such that volumetric distortion is controlled in the simulation. Typically, adjusting K to be an order of magnitude greater than the maximum stress experienced by the model provides transient volumetric strains of less than 1%.

As noted earlier, a Lagrangian solution is required in order to update the unit vectors tracking the platelet fiber direction and normal directions resulting from the deformation gradient. In early investigations of Jeffery's equations, a Lagrangian description of fiber orientation state was achieved by integrating along streamlines [37] while the flow solution was computed in a Eulerian framework. Herein, a Lagrangian description of platelet orientations is achieved by using the SPH method [38,39] implemented in ABAQUS 2016 [40]. The SPH method is meshfree allowing extreme deformations required by mold filling. By using the same integration points for the orientation state and the flow solution, some fidelity in orientation state scale may be sacrificed if the integration point density cannot match or exceed the platelet number density.

For the considered molded bracket geometry [Fig. 1(c)], a particle domain is created with 12 layers of 12 716 particles per layer for a total of 152 592 PC3D elements as shown in Fig. 7. As an explicit solution is used, the stable time increment for the simulation depends upon the tangent modulus, material density, and characteristic element dimension. PPMCs as modeled herein behave with large viscosity and near incompressibility resulting in a large tangent modulus. The platelet system is of low density and platelets are of a relatively thin dimension. All of these characteristics seek to lower the stable time increment. Thus, the following simulation is performed utilizing manual mass scaling and the relatively coarse discretization mentioned to achieve acceptable computation times. Finally, the solution is computed under a zero traction boundary condition at the bounding surfaces (i.e., pure slip). While typical fluid mechanics calculations are performed with no-slip boundary conditions, Tucker [34] notes in an order of magnitudes analysis for suspension flow

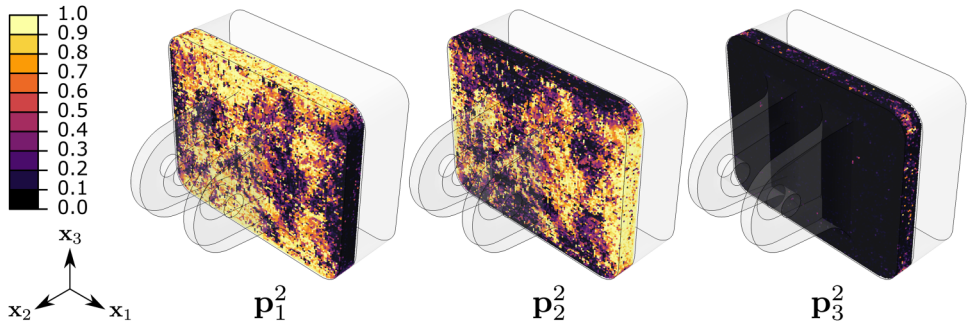

FIG. 7. Initial fiber directions (components squared): measured from CT scan and initialized on SPH domain for flow simulation.

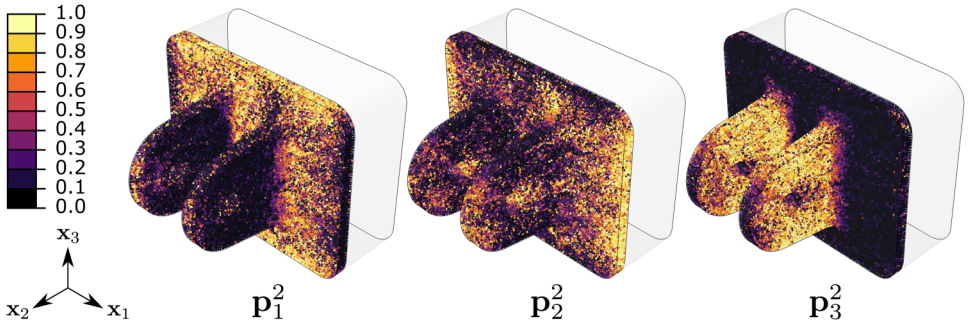

FIG. 8. Final fiber directions (components squared): predicted by flow simulation. Multimedia view (movie: compression molding simulation): https://doi.org/10.1122/1.5044533.1.

in narrow gaps that for sheet molding compounds (SMC) and SMC-like materials with large degrees of anisotropy and highly planar orientation states, a thin boundary layer may form with the bulk of the material experiencing plug-flow or a zero traction boundary condition. However, in the present case, to capture the development of such a boundary layer would require significantly increased particle density, thereby resulting in intractable computation conditions.

In detail, due to the use of Newtonian viscosity, the simulated rate and absolute viscosity magnitude are unimportant. Therefore, the molding process is treated as occurring in 1 s and the neat matrix viscosity is taken as $\eta_0 = 1$ Pa s. As the stable time increment of explicit simulation scales with $\sqrt{\rho}$, the material density is treated variably as

$$\rho = 1.60 \times 10^n \ \mathrm{g/mm^3}, \tag{10}$$

where n is chosen as large as possible while still maintaining a relatively low Reynolds number with the physical material having $n \approx -3$. In the absence of no-slip boundary conditions, the primary deformation mode experienced by the material is in-plane stretching. The flow in the base of the pin bracket is primarily lubricated squeeze flow. The velocity of the ram is 3.55 mm/s, and the initial height of the base is 6.00 mm. For lubricated squeeze flow ($\mathbf{D}_{33} = -\dot{\varepsilon}$ and $\mathbf{D}_{11} = \mathbf{D}_{22} = \dot{\varepsilon}/2$) and a quasi-isotropic orientation state, the effective viscosity is given as

$$\eta^{\mathrm{eff}} \approx \boldsymbol{\sigma}_{33}/\mathbf{D}_{33} = (R_\eta + 2)\eta_{23} = (R_\eta + 2)\kappa\eta_0, \tag{11}$$

where $\kappa = 5.36$ for $V_f = 0.60$ according to the theory of Pipes *et al.* [28]. Upon substitution, the Reynolds number is approximated as

$$\mathrm{Re} \approx \frac{6.36 \times 10^n}{R_\eta + 2}. \tag{12}$$

For creeping flow, we require the Reynolds number to be low, $\mathrm{Re} \ll 1$. As a maximum limit, consider $\mathrm{Re} = 0.01$. For this case, with the anisotropy ratio used in the present simulation, $R_\eta = 61\,215$, the density exponent is determined as $n \approx 2$. In the presented result, $n = 1$ is used. Finally, through performing the simulation and adjusting the penalizing bulk modulus based on observed volumetric strain, $K = 1.31$ GPa was found to appropriately control the volumetric strain through filling (i.e., kept the mean volumetric strain below 1%). The simulations were performed using ABAQUS 2016 on Purdue University's Halstead cluster on one node with 20 cores and took 22 h to complete in $\sim 7 \times 10^5$ increments with an average time step of $\sim 1.5 \times 10^{-6}$ s.

IV. RESULTS AND DISCUSSION

The initial orientation state determined from the CT scan analysis is mapped to the SPH particle elements through a nearest-neighbor mapping. For each particle element, the orientation state determined at the nearest element of the CT scan data is taken as the orientation state of the particle element. Interpolation based mapping is not used due to the tracking of orientation vectors which lack algebraic averaging. This procedure captures the in-charge-plane fidelity of the platelets well; however, there is some loss of through-thickness orientation information as only 12 layers are used in the SPH domain. The resulting orientation state of the

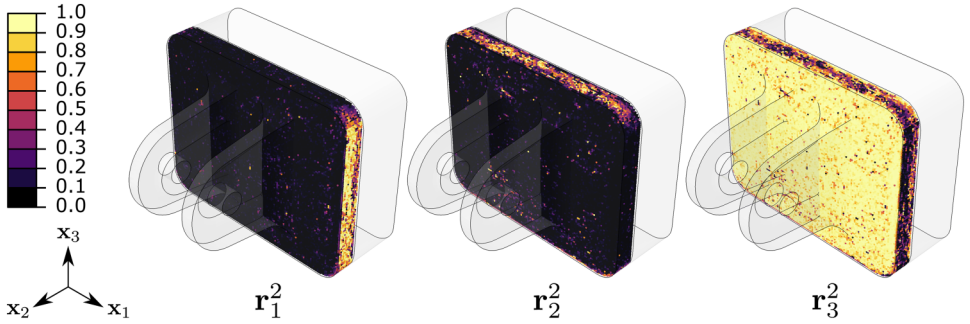

FIG. 9. Initial platelet normal directions (components squared): measured from CT scan and initialized on SPH domain for flow simulation.

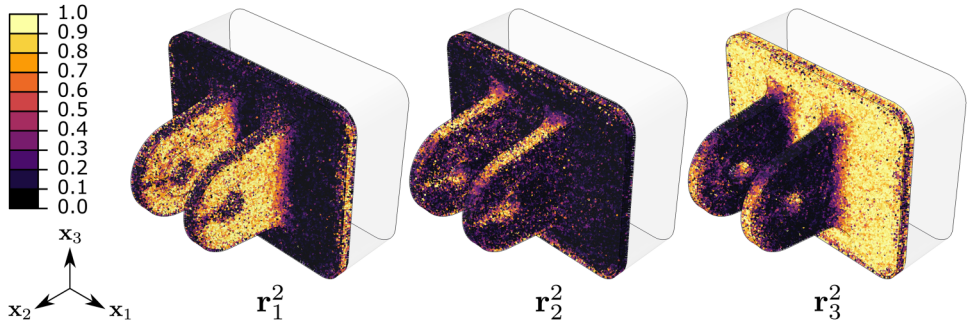

FIG. 10. Final platelet normal directions (components squared): predicted by flow simulation. Multimedia view (movie: compression molding simulation): https://doi.org/10.1122/1.5044533.2

initial charge is shown in Fig. 7 (fiber direction) and Fig. 9 (normal direction) using the square of the vector components. Additionally, the charge averaged, second-order, fiber orientation tensor and normal orientation tensor are given as

$$\mathbf{A} = \begin{bmatrix} 0.503 & -0.015 & 0.027 \\ -0.015 & 0.469 & -0.003 \\ 0.027 & -0.003 & 0.028 \end{bmatrix}, \qquad \mathbf{N} = \begin{bmatrix} 0.071 & 0.001 & -0.045 \\ 0.001 & 0.088 & 0.001 \\ -0.045 & 0.001 & 0.841 \end{bmatrix}, \tag{13}$$

where a planar uniform orientation state has terms $\mathbf{A}_{11} = \mathbf{A}_{22} = 1/2$ and $\mathbf{N}_{33} = 1$ with all others zero. From the initial state, we see that platelets tend to align with the lateral boundaries of the mold during the pouring and consolidation stages. Also, at the lateral tool boundaries, some platelets turn so that their normal direction is nearly parallel to the nearest tool normal rather than normal to the charge plane. Due to the greater length of lateral boundaries in the $\mathbf{x}_1$-direction, the charge average orientation state is slightly aligned in the $\mathbf{x}_1$-direction ($\mathbf{A}_{11} > \mathbf{A}_{22}$).

With the preform initial orientation state fully characterized, the flow simulation was carried out and the resulting orientation states (vector components squared) from the flow simulation are shown in Figs. 8 and 10 (Multimedia view). The flow and orientation state progressing from Figs. 7 to 8 (Multimedia view; for the fiber direction) and from Figs. 9 to 10 (Multimedia view; for the normal direction) can be seen in the online article. Here, the material stretching to fill the flanges of the molded geometry greatly increased the degree of orientation along the $\mathbf{x}_3$-direction, $\mathbf{A}_{33}$, in the flanges, while the material stretching in the base increased the $\mathbf{x}_1$-direction alignment. Additionally, the effect of the molded-in hole is shown to generate large $\mathbf{A}_{22}$ below the hole. However, as the two flow fronts diverge around the hole and then reconnect, a knit-line is formed, resulting in low $\mathbf{A}_{22}$ that indicates no reinforcement crossing the knit-line. Additionally, while the platelet normal directions in the flanges are parallel to the flange normal, near the knit-line, the platelet normals cross the knit-line (large $\mathbf{N}_{22}$).

Due to the highly heterogeneous nature of the molded microstructure, it is difficult to perform a point to point comparison between any two orientation results for PPMCs regardless of the source of the orientation information.

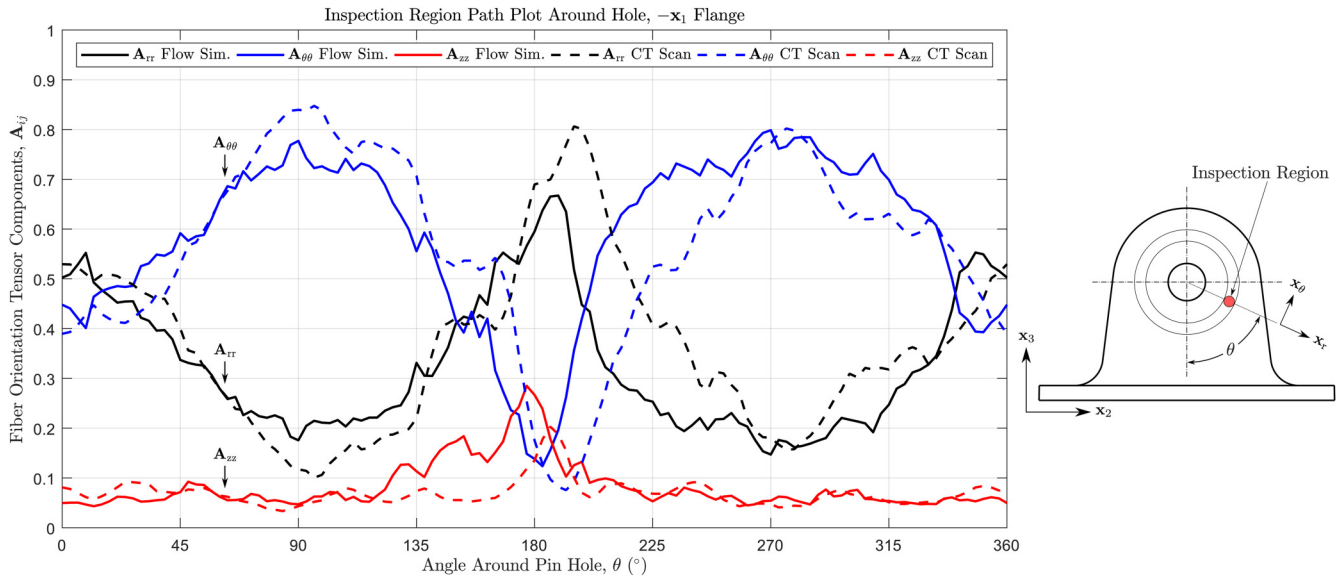

FIG. 11. Inspection region path plot, fiber direction orientation tensor components, $-\mathbf{x}_1$ flange.

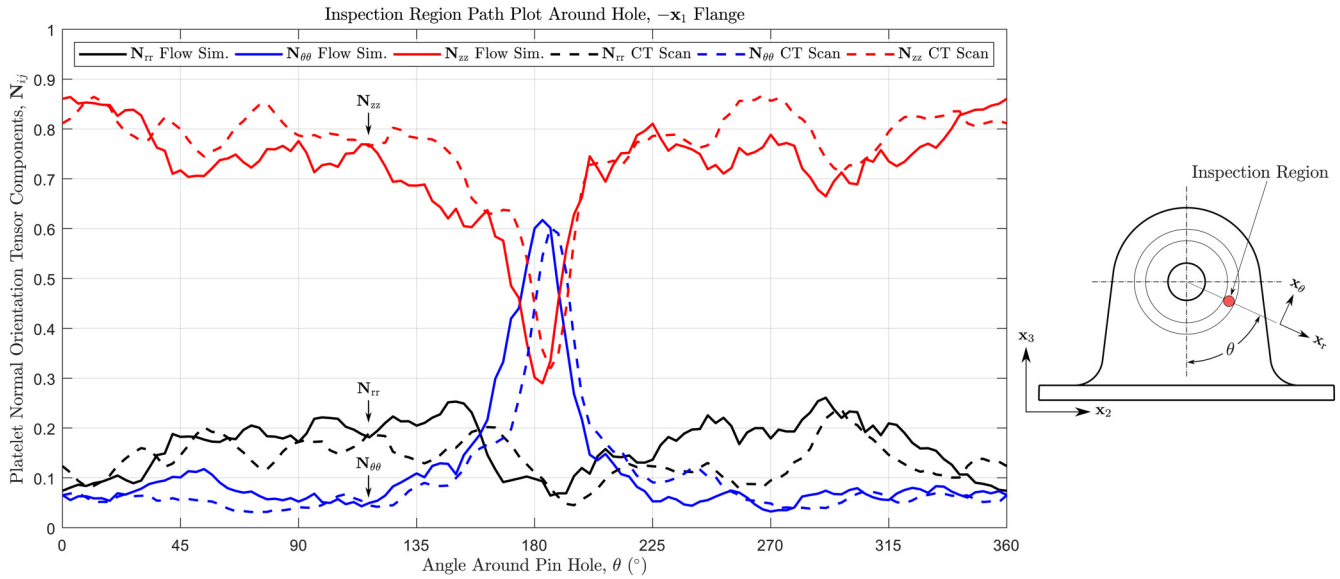

FIG. 12. Inspection region path plot, platelet normal orientation tensor components, $-\mathbf{x}_1$ flange.

Therefore, to perform comparisons, a local orientation average about a given point was performed. Each point along a path is treated as the center of an inspection region and the volume-averaged orientation tensors in that region is computed. For the bracket geometry, the variation of the orientation state around the molded-in hole is particularly interesting. In Figs. 11 and 12, the variation of the fiber orientation tensor and the platelet normal orientation tensor in the inspection region is shown for the region around the molded-in hole in cylindrical coordinates. Here, the predictions vary similar to the CT scan determined results. In particular, the region above the pin hole ($\theta \approx 180°$), where one should expect to see an orientation structure indicating the knit-line, a relatively low $\mathbf{A}_{\theta\theta}$ and large $\mathbf{A}_{rr}$ indicate that fibers are pointing radially and a relatively high $\mathbf{N}_{\theta\theta}$ indicates that platelet normals are pointing across the knit-line. Additionally, in the region directly below the hole ($\theta \approx 0°$), a relatively large $\mathbf{A}_{\theta\theta}$ indicates that as the material stretches in the $\mathbf{x}_\theta$-direction to flow around the pin hole, platelets orient in this stretching direction. However, the platelet normal orientation state is relatively uniform throughout the entire path and parallel to the flange surface normal directions, except at the knit-line.

Another comparison is performed to examine the variation of orientation state in the base of the bracket along the $\mathbf{x}_1$-direction. In Figs. 13 and 14, the variation of the fiber orientation tensor components and the platelet normal orientation tensor components are shown along the base. Each point represents an average through the full base thickness, across the full base width for 50 equally sized slices along the $\mathbf{x}_1$-direction. Here, the trends of the orientation state in the base are captured well, though less agreement is seen directly below the flanges. The flow simulation predicts that the platelets are stretched in the $\mathbf{x}_1$-direction in order to flow into the

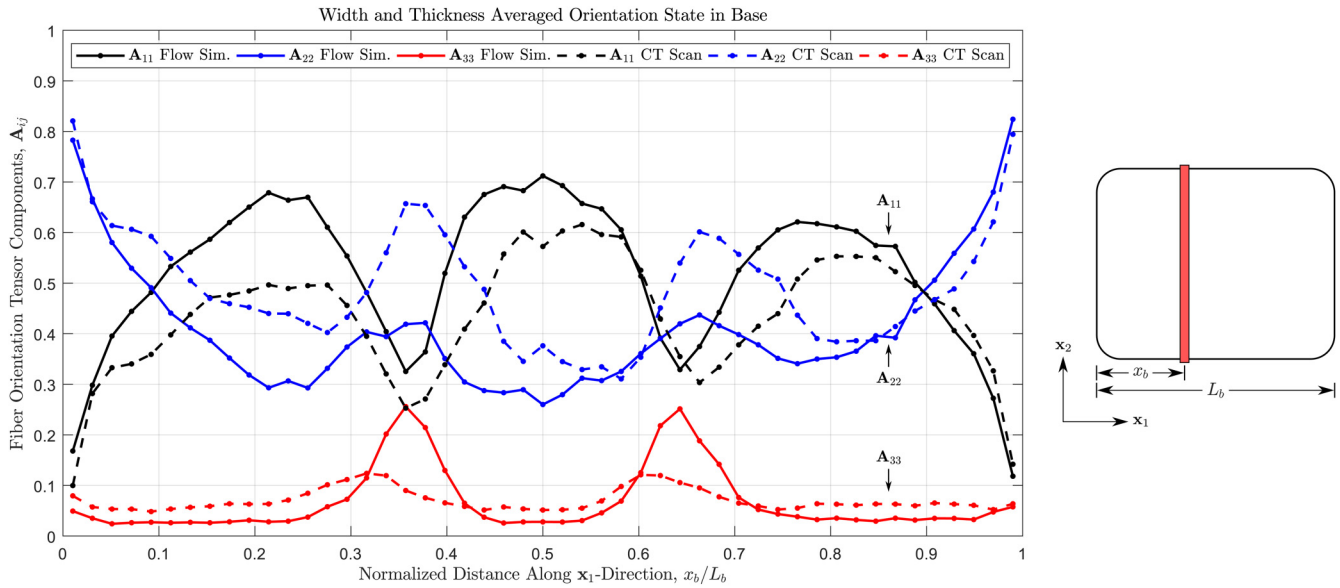

FIG. 13. Width and thickness averaged fiber orientation tensor components in base.

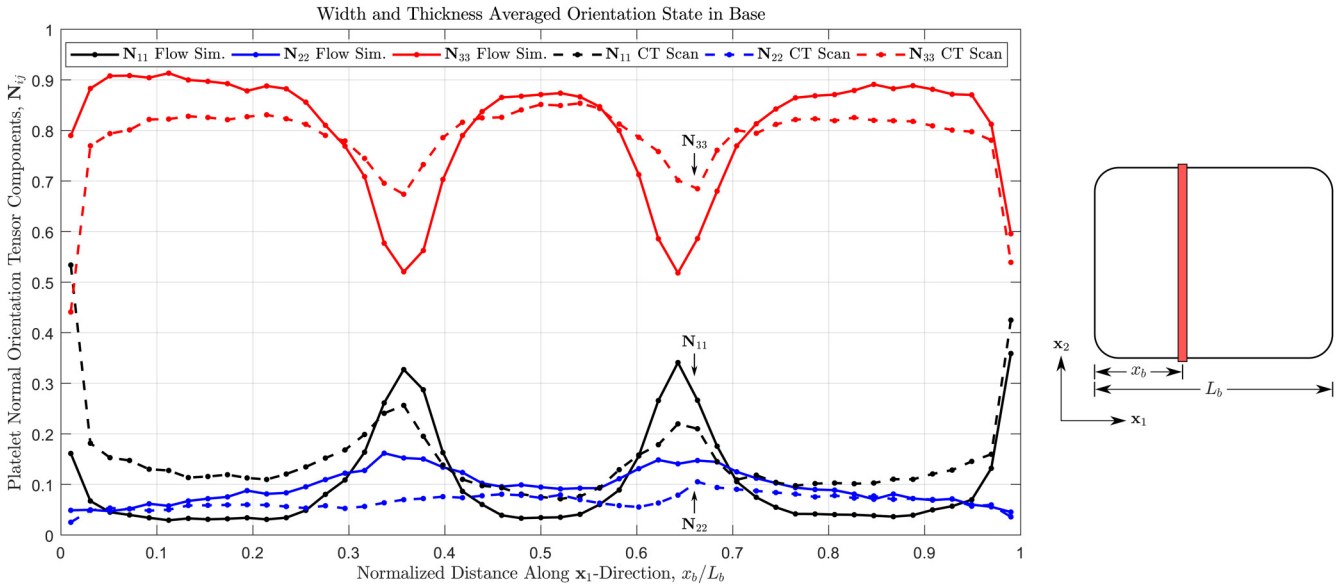

FIG. 14. Width and thickness averaged platelet normal orientation tensor components in base.

flanges then turn into the $\mathbf{x}_3$-direction upon entering the base of the flange, while the CT scan result seems to indicate that the $\mathbf{A}_{22}$ is quite large directly below the flange. Physically, this behavior could be due to complex boundary interactions between platelets and boundaries such that platelets are forced to turn into an orientation that is geometrically preferred by the flange entrance. For short-fiber suspensions, such interactions have been explored by Schiek and Shaqfeh [41] using a nonlocal constitutive model for flow in a confined channel. In the present investigation, these effects cannot be captured due to the inherent assumption and modeling simplification of continuum flow.

V. CONCLUSIONS

In this work, the authors have developed, implemented, and validated a new method for performing flow simulation of PPMCs. In particular, a fully coupled anisotropic flow and orientation analysis method was developed in ABAQUS/EXPLICIT using the SPH method and user subroutines such that both fiber directions and platelet normal directions are predicted during flow. The use of orientation vectors as primary variables rather than orientation tensor and a Lagrangian numerical framework were key considerations to capture and maintain the spatial variability of PPMCs through molding. A validation exercise was performed in which a material charge was preconsolidated, its orientation state was determined with CT scan methods, a flow simulation was performed with the determined orientations as the initial state, and a final molded geometry was produced and CT scanned using the material charge. Comparisons between orientation states have shown strong agreement between predictions and experimental measurements in much of the molded geometry. However, strong $\mathbf{x}_2$-direction alignment at the entrance to the flanges in the base was not captured as strongly in the simulation and is likely due to larger scale interactions between platelets and tool boundaries.

ACKNOWLEDGMENTS

This material is based upon work supported by the National Science Foundation Graduate Research Fellowship Program under Grant No. DGE-1333468. Any opinions, finding, and conclusions or recommendations expressed in this material are those of the authors and do not necessarily reflect the views of the National Science Foundation. This work was sponsored by the Boeing Company under Master Agreement No. 2011-042.

NOMENCLATURE

$\mathbf{A} = \langle \mathbf{pp} \rangle$	second-order fiber orientation tensor
$\mathbb{A} = \langle \mathbf{pppp} \rangle$	fourth-order fiber orientation tensor
$\mathbf{D} = (\mathbf{L} + \mathbf{L}^T)/2$	rate-of-deformation tensor
D_f	fiber diameter
$\mathbf{F} = \mathbf{F}_{ij} = \partial \mathbf{x}_i / \partial \mathbf{x}_j^0$	deformation gradient tensor
F	maximum packing fraction, $F = \pi/\sqrt{12}$ for hexagonal packing
H	platelet thickness
K	bulk modulus
$\mathbf{L} = \dot{\mathbf{F}} \cdot \mathbf{F}^{-1} = \mathbf{W} + \mathbf{D}$	velocity gradient tensor
L	platelet length
L_f	fiber length
$\mathbf{N} = \langle \mathbf{rr} \rangle$	second-order platelet normal orientation tensor
$\mathbb{N} = \langle \mathbf{rrrr} \rangle$	fourth-order platelet normal orientation tensor
P	pressure
$\mathbf{p}$	platelet fiber direction
$\mathbf{p}^0$	initial fiber

$\mathbf{q}$	orthogonal in-plane direction
$\hat{\mathbf{q}}$	nonorthogonal in-plane direction
$\mathbf{q}^0$	in-plane transverse
Re	Reynold's number
$R_\eta = \eta_{11}/\eta_{22} = (\eta_{11}/\eta_{23} + 1)/4$	dimensionless anisotropy ratio
$\mathbf{r}$	platelet normal direction
$\mathbf{r}^0$	platelet normal directions
t	time
V_f	volume fraction
$\mathbf{W} = (\mathbf{L} - \mathbf{L}^T)/2$	vorticity tensor
W	platelet width
$\mathbf{x}$	current coordinate
$\mathbf{x}^0$	initial coordinate

Greek

$\Delta\varepsilon$	strain increment
Δt	time increment
η_0	neat resin viscosity
η_{11}	extensional viscosity in the fiber direction
η_{12}	in-plane shearing viscosity
η_{23}	transverse shearing viscosity
$\kappa = 1/\left(1 - \sqrt{V_f/F}\right)$	fiber volume fraction parameter
$\boldsymbol{\tau}$	deviatoric stress tensor
$\boldsymbol{\sigma}$	stress tensor
ρ	density

APPENDIX

To assist in understanding the proposed model for fiber direction and normal direction evolution and to demonstrate the platelet normal orientation model, one can observe the behavior of the model in a simple case with the orientation field solved using tensor methods. For large geometries (relative to platelet scale), it may be desirable to resort to tensor-based methods to reduce computational expense and provide a more appropriate orientation result. In orientation tensor form, Eqs. (3) and (4) are transformed to Eqs. (A1) and (A2):

$$\dot{\mathbf{A}} = \mathbf{W}\cdot\mathbf{A} - \mathbf{A}\cdot\mathbf{W} + (\mathbf{D}\cdot\mathbf{A} + \mathbf{A}\cdot\mathbf{D} - 2\mathbf{D}:\mathbb{A}), \tag{A1}$$

$$\dot{\mathbf{N}} = \mathbf{W}\cdot\mathbf{N} - \mathbf{N}\cdot\mathbf{W} - (\mathbf{D}\cdot\mathbf{N} + \mathbf{N}\cdot\mathbf{D} - 2\mathbf{D}:\mathbb{N}), \tag{A2}$$

where $\mathbf{A} = \langle\mathbf{pp}\rangle$ and $\mathbb{A} = \langle\mathbf{pppp}\rangle$ are the second- and fourth-order fiber orientation tensors and $\mathbf{N} = \langle\mathbf{rr}\rangle$ and $\mathbb{N} = \langle\mathbf{rrrr}\rangle$ are the second- and fourth-order platelet normal orientation tensors, respectively. With the second-order tensors as the primary variables, the fourth-order tensors must be approximated by a closure approximation. For this investigation, the natural closure of Verleye *et al.* [42] as given by VerWeyst [43] for the fourth-ordered fiber orientation tensor, $\mathbb{A}$, is used. However, closure approximations have typically been determined for fiber suspensions using Eq. (A1) or the Folgar–Tucker model, not for Eq. (A2). Fortunately, this is not an issue if the method by which closure approximations are generated is considered. Typically, a fitted closure approximation is determined by subjecting an initially 3D uniform orientation state to a set of flow fields, different velocity gradients $\mathbf{L}$, using orientation distribution function methods such that the so-called orientation triangle is well-covered by the resulting data points [44]. The resulting data points which correlate a determined second-order orientation tensor and a fourth-order orientation tensor are used to fit polynomial functions in terms of the orientation tensor eigenvalues [44] or invariants [45]. Provided an initially 3D uniform orientation state, it can be seen from the form of Eq. (A2) that the same data points determined using Eq. (A1) and $\mathbf{L} = \mathbf{W} + \mathbf{D}$ would be determined using $-\mathbf{L}^{\mathrm{T}} = \mathbf{W} - \mathbf{D}$. Thus, the same fitting points would be determined under slightly modified velocity fields. For example, evolving the fiber orientation state with Eq. (3) and

$$\mathbf{L} = \begin{bmatrix} 0 & 0 & \dot{\gamma} \\ 0 & 0 & 0 \\ 0 & 0 & 0 \end{bmatrix}, \tag{A3}$$

and evolving the platelet normal orientation state with Eq. (4) and

$$\mathbf{L} = \begin{bmatrix} 0 & 0 & 0 \\ 0 & 0 & 0 \\ -\dot{\gamma} & 0 & 0 \end{bmatrix}, \tag{A4}$$

provide equivalent data points for fitting a closure approximation. The natural closure is formed using exact solutions of the distribution function under a given deformation gradient. Similarly, forming the orientation distribution for the fiber orientation using Eq. (A5)

$$\mathbf{F} = \begin{bmatrix} 1 & 0 & \gamma \\ 0 & 1 & 0 \\ 0 & 0 & 1 \end{bmatrix}, \tag{A5}$$

provides equivalent fitting points as forming the orientation

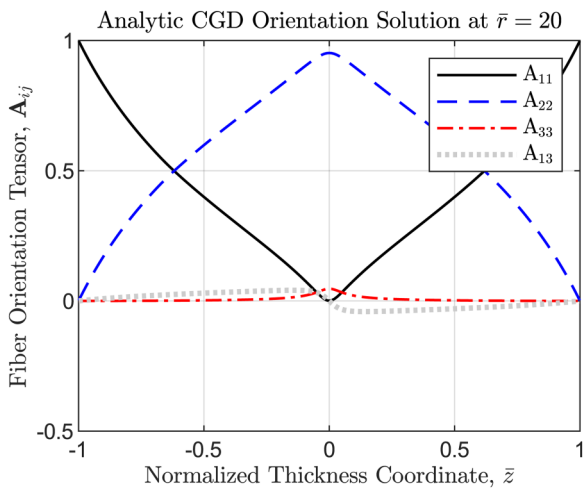

FIG. 15. Analytic CGD fiber orientation tensor solution.

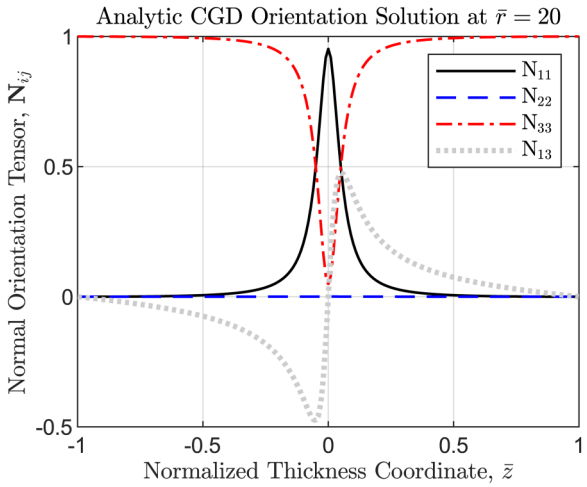

FIG. 16. Analytic CGD normal orientation tensor solution.

distribution for the platelet normal using Eq. (A6)

$$\mathbf{F} = \begin{bmatrix} 1 & 0 & 0 \\ 0 & 1 & 0 \\ -\gamma & 0 & 1 \end{bmatrix}. \tag{A6}$$

In this way, it is clear that for Jeffery's equation without diffusion effects, the closure approximation formed for $\mathbb{N}$ would be equivalent to that formed for $\mathbb{A}$. Similarly, closures formed for fiber orientations under isotropic diffusion are equivalent to those formed for $\mathbb{N}$ under isotropic diffusion. Thus, herein, we use the natural closure approximation for $\mathbb{A}$ as a function of $\mathbf{A}$ and for $\mathbb{N}$ as a function of $\mathbf{N}$.

Altan and Rao [46] solved for the analytical velocity field in a CGD considering an isothermal, isotropic, and Newtonian viscosity. The velocity gradient is given by

$$\mathbf{L} = \bar{Q}\begin{bmatrix} -(1-\bar{z}^2)/\bar{r}^2 & 0 & -2\bar{z}/\bar{r} \\ 0 & (1-\bar{z}^2)/\bar{r}^2 & 0 \\ 0 & 0 & 0 \end{bmatrix}, \tag{A7}$$

where $\bar{Q}$ is a normalized flow rate, $\bar{r}$ is a normalized radial coordinate, and $\bar{z}$ is a normalized thickness coordinate. This velocity field is interesting in that near the boundaries, $|\bar{z}| = 1$, simple shear is encountered, near the midplane, $\bar{z} = 0$, planar extension is encountered, and at intermediate points, both shear and extension are encountered with varying weights. Thus, the velocity gradient provides a simple way to assess the behavior of the orientation model under a range of deformation modes. Using the velocity gradient and an initial orientation state assumed here to be 3D uniform random (i.e., $\mathbf{A} = \mathbf{N} = \mathrm{I}/3$), the orientation state through the thickness at a given radial coordinate can be determined. In Figs. 15 and 16, the resulting fiber orientation tensor components and platelet normal orientation tensors components, respectively, at $\bar{r} = 20$ are shown. Here, it can be seen that while the fiber orientation tensor shows flow alignment (large $\mathbf{A}_{11}$) in the shell region near the boundaries varying to transverse alignment (large $\mathbf{A}_{22}$) in the core region near the midplane, the platelet normal orientation tensor shows large $\mathbf{N}_{33}$ throughout nearly the entire thickness except for a very small portion near the midplane. These results indicate that the fiber directions have flattened to lie primarily in the $\mathbf{x}_1$–$\mathbf{x}_2$ plane with the normals similarly collapsed into the $\mathbf{x}_3$-direction.

This short investigation confirms the ability to use orientation tensor-based methods for both the fiber direction and the platelet normal direction using the same closure approximation and demonstrates the difference in resulting tensor components seen in a simple analytic flow. While not shown in detail, diffusion models [15] including anisotropic diffusion [16–18] and reduced orientation kinetic models [20,21] can be expressed in addition to Eq. (A2) if found to be desirable behavior for the evolution of the normal orientation tensor.

References

[1] Pipes, R. B., R. L. McCullough, and D. G. Taggart, "Behavior of discontinuous fiber composites: Fiber orientation," Polym. Compos. **3**, 34–39 (1982).

[2] Landry, B., and P. Hubert, "Experimental study of defect formation during processing of randomly-oriented strand carbon/PEEK composites," Compos. Part A Appl. Sci. Manuf. **77**, 301–309 (2015).

[3] LeBlanc, D., B. Landry, A. Levy, P. Hubert, S. Roy, A. Yousefpour, and E. Quinlan, "Study of processing conditions on the forming of ribbed features using randomly oriented strands thermoplastic composites," J. Am. Helicopter Soc. **60**, 1–9 (2015).

[4] Visweswaraiah, S. B., M. Selezneva, L. Lessard, and P. Hubert, "Mechanical characterisation and modelling of randomly oriented strand architecture and their hybrids – a general review," J. Reinf. Plast. Compos. **37**, 548–580 (2018).

[5] Kravchenko, S. G., Failure analysis in platelet molded composite systems, Ph.D. thesis, Purdue University, West Lafayette, IN, 2017.

[6] Selezneva, M., G.-P. Picher-Martel, B. Landry, L. Lessard, P. Hubert, D. Trudel-Boucher, L. Khoun, S. Roy, and M. Hojjati, "Compression moulding of discontinuous-fibre carbon/PEEK composites: Study of mechanical properties," *International SAMPE Technical Conference*, Baltimore, MD, 2012.

[7] Picher-Martel, G. P., A. Levy, and P. Hubert, "Compression molding of carbon/polyether ether ketone composites: Squeeze flow behavior of unidirectional and randomly oriented strands," Polym. Compos. **38**, 1828–1837 (2017).

[8] Levy, A., and P. Hubert, "Interstrand void content evolution in compression moulding of randomly oriented strands (ROS) of thermoplastic composites," Compos. Part A Appl. Sci. Manuf. **70**, 121–131 (2015).

[9] Picher-Martel, G.-P., A. Levy, and P. Hubert, "Compression moulding of carbon/PEEK randomly-oriented strands composites: A 2D finite element model to predict the squeeze flow behaviour," Compos. Part A Appl. Sci. Manuf. **81**, 69–77 (2016).

[10] Denos, B. R., S. G. Kravchenko, and R. B. Pipes, "Progressive failure analysis in platelet based composites using CT-measured local microstructure," *International SAMPE Technical Conference*, Seattle, WA (Society for the Advancement of Material and Process Engineering, 2017), pp. 1421–1435.

[11] Denos, B. R., Fiber orientation measurements in platelet-based composites via computed tomography analysis, Ph.D. thesis, Purdue University, West Lafayette, IN, 2017.

[12] Sommer, D. E., A. J. Favaloro, and R. B. Pipes, "Coupling anisotropic viscosity and fiber orientation in applications to squeeze flow," J. Rheol. **62**, 669 (2018).

[13] Denos, B. R., D. E. Sommer, A. J. Favaloro, R. B. Pipes, and W. B. Avery, "Fiber orientation measurement from mesoscale CT scans of prepreg platelet molded composites," Compos. Part A Appl. Sci. Manuf. **114**, 241–249 (2018).

[14] Jeffery, G. B., "The motion of ellipsoidal particles immersed in a viscous fluid," Proc. R. Soc. A Math. Phys. Eng. Sci. **102**, 161–179 (1922).
[15] Folgar, F., and C. L. Tucker, "Orientation behavior of fibers in concentrated suspensions," J. Reinf. Plast. Compos. **3**, 98–119 (1984).
[16] Phelps, J. H., and C. L. Tucker, "An anisotropic rotary diffusion model for fiber orientation in short- and long-fiber thermoplastics," J. Non-Newtonian Fluid Mech. **156**, 165–176 (2009).
[17] Tseng, H.-C., R.-Y. Chang, and C.-H. Hsu, "An objective tensor to predict anisotropic fiber orientation in concentrated suspensions," J. Rheol. **60**, 215–224 (2016).
[18] Tseng, H.-C., R.-Y. Chang, and C.-H. Hsu, "The use of principal spatial tensor to predict anisotropic fiber orientation in concentrated fiber suspensions," J. Rheol. **62**, 313–320 (2018).
[19] Huynh, H. M., Improved fiber orientation prediction for injection molded composites, Ph.D. thesis, University of Illinois at Urbana-Champaign, 2001).
[20] Wang, J., J. F. O'Gara, and C. L. Tucker, "An objective model for slow orientation kinetics in concentrated fiber suspensions: Theory and rheological evidence," J. Rheol. **52**, 1179–1200 (2008).
[21] Tseng, H.-C., R.-Y. Chang, and C.-H. Hsu, "Phenomenological improvements to predictive models of fiber orientation in concentrated suspensions," J. Rheol. **57**, 1597–1631 (2013).
[22] Tucker, C. L., and S. G. Advani, "Processing of short-fiber systems," *Flow and Rheology in Polymer Composites Manufacturing* (1994), Vol. 10, Chap. 6, pp. 147–203.
[23] Hinch, E. J., and L. G. Leal, "Constitutive equations in suspension mechanics. Part 2. Approximate forms for a suspension of rigid particles affected by Brownian rotations," J. Fluid Mech. **76**, 187–208 (1976).
[24] Advani, S. G., and C. L. Tucker, "The use of tensors to describe and predict fiber orientation in short fiber composites," J. Rheol. **31**, 751–784 (1987).
[25] Batchelor, G. K., "The stress generated in a non-dilute suspension of elongated particles by pure straining motion," J. Fluid Mech. **46**, 813–829 (1971).
[26] Dinh, S. M., and R. C. Armstrong, "A rheological equation of state for semiconcentrated fiber suspensions," J. Rheol. **28**, 207–227 (1984).
[27] Shaqfeh, E. S. G., and G. H. Fredrickson, "The hydrodynamic stress in a suspension of rods," Phys. Fluids A **2**, 7–24 (1990).
[28] Pipes, R. B., D. W. Coffin, P. Simacek, S. F. Shuler, and R. K. Okine, "Rheological behavior of collimated fiber thermoplastic composite materials," *Flow and Rheology in Polymer Composites Manufacturing* (1994), Vol. 10, Chap. 4, pp. 85–125.
[29] Favaloro, A. J., Rheological behavior and manufacturing simulation of Prepreg platelet molding systems, Ph.D. thesis, Purdue University, West Lafayette, IN, 2017.
[30] Sommer, D. E., Constitutive modeling of the rheological behavior of platelet suspensions, M.S.A.A thesis, Purdue University, West Lafayette, IN, 2016.
[31] Beaussart, A. J., J. W. S. Hearle, and R. B. Pipes, "Constitutive relationships for anisotropic viscous materials," Compos. Sci. Technol. **49**, 335–339 (1993).
[32] Sundararajakumar, R. R., D. L. Koch, and E. S. G. Shaqfeh, "The extensional viscosity and effective thermal conductivity of a dispersion of aligned disks," Phys. Fluids **6**, 1955–1962 (1994).
[33] Loredo, A., and H. Klöcker, "Generalized inverse of the compliance tensor, and behaviour of incompressible anisotropic materials—application to damage," Mech. Res. Commun. **24**, 371–376 (1997).
[34] Tucker, C. L., "Flow regimes for fiber suspensions in narrow gaps," J. Non-Newtonian Fluid Mech. **39**, 239–268 (1991).
[35] Ericsson, K. A., S. Toll, and J.-A. E. Manson, "The two-way interaction between anisotropic flow and fiber orientation in squeeze flow," J. Rheol. **41**, 491–511 (1997).
[36] Song, Y., U. Gandhi, C. Pérez, T. Osswald, S. Vallury, and A. Yang, "Method to account for the fiber orientation of the initial charge on the fiber orientation of finished part in compression molding simulation," Compos. Part A Appl. Sci. Manuf. **100**, 244–254 (2017).
[37] Givler, R. C., M. J. Crochet, and R. B. Pipes, "Numerical prediction of fiber orientation in dilute suspensions," J. Compos. Mater. **17**, 330–343 (1983).
[38] Gingold, R. A., and J. J. Monaghan, "Smoothed particle hydrodynamics: Theory and application to non-spherical stars," Mon. Not. R. Astron. Soc. **181**, 375–389 (1977).
[39] Liu, G. R., and M. B. Liu, *Smoothed Particle Hydrodynamics: A Meshfree Particle Method* (World Scientific, Singapore, 2003).
[40] ABAQUS. Abaqus 2016 Documentation, 2016.
[41] Schiek, R. L., and E. S. G. Shaqfeh, "A nonlocal theory for stress in bound, Brownian suspensions of slender, rigid fibres," J. Fluid Mech. **296**, 271–324 (1995).
[42] Verleye, V., A. Couniot, and F. Dupret, "Numerical prediction of fiber orientation in complex composite injection-molded parts," *ASME Winter Annual Meeting*, Chicago IL (ASME Heat Transfer Division (HTD) and ASME Material Division (MD), 1994), Vols. 289 and 48, pp. 265–279.
[43] VerWeyst, B. E., Numerical predictions of flow-induced fiber orientation in three-dimensional geometries, Ph.D. thesis, University of Illinois at Urbana-Champaign, 1998.
[44] Cintra, J. S., and C. L. Tucker III, "Orthotropic closure approximations for flow-induced fiber orientation," J. Rheol. **39**, 1095–1122 (1995).
[45] Chung, D. H., and T. H. Kwon, "Invariant-based optimal fitting closure approximation for the numerical prediction of flow-induced fiber orientation," J. Rheol. **46**, 169–194 (2002).
[46] Altan, M. C., and B. N. Rao, "Closed-form solution for the orientation field in a center-gated disk," J. Rheol. **39**, 581–599 (1995).